PHYSICAL REVIEW APPLIED 20, 044022 (2023)
DOI: 10.1103/PhysRevApplied.20.044022

Current-controlled memristors: resistive switching systems with negative capacitance and inverted hysteresis

Juan Bisquert[1]*
[1]Institute of Advanced Materials (INAM), Universitat Jaume I, 12006 Castelló, Spain

Corresponding author Email: bisquert@uji.es

Abstract

Resistive switching in memristors is being amply investigated for different applications in non-volatile memory (RRAM), neuromorphic computing and programmable logic devices. Memristors are conducting devices in which the conductance depends on one or more slow internal state variables, and they exhibit strongly nonlinear properties and intense memory effects. Here we address the characterization of current-controlled memristors by small perturbation frequency-resolved impedance techniques. We show that the equivalent circuit obtained at different stationary points provides essential information of the dynamical behaviour in voltage cycling and transient response to a square perturbation. The general method enables the analysis of stability and hysteresis in current-voltage curves. The current-controlled memristor produces very naturally a negative capacitance effect, and we review several devices in the literature, including discharge tubes and metal-oxide memristors, to expose the deep connections between the sign of the capacitance and the type of hysteresis.

1. Introduction

Resistive switching is a phenomenon where certain materials change their resistance in response to an electrical stimulus. It has applications in non-volatile memory (RRAM), neuromorphic computing, programmable logic devices, analog computing, sensors, energy storage, and radiation detection. These applications offer benefits in high-density storage, low power consumption, fast switching speeds, and potential advancements in various fields.

Resistive switching systems have been investigated for centuries and ongoing research continues to explore and expand the potential of resistive switching technology [1-3]. In recent decades [4] these systems have been broadly conceptualized as memristors, following Chua's suggestion [5,6]. Memristors can be defined as a nonlinear system with memory affected by one or more state variables denoted x_i [7]. These x_i are variables necessary to determine the future behaviour of a system when the present state and the inputs are known. Consider two complementary conjugate electrical variables Z, Y (meaning voltage u, current I, charge or flux). The most basic model of a memristor satisfies a structural set of equations of the type [5]

$$Y = F(Z, x_i) \tag{1}$$

$$\tau_{k,i} \frac{dx_i}{dt} = g_i(Z, x_i) \tag{2}$$

The first equation is a generalized conductance. But by the dependence on x the variable Y does not respond instantaneously to the changes of stimulus Z . The changes of the "slow" state variable x are controlled by a driven adaptation function $g(Z, x)$ with the characteristic time τ_k.

Resistive switching in memristors occurs by a threshold of voltage or current, as shown in Fig. 1a. An external bias causes a modification of a high resistance state to a low resistance state, and the initial state can be restored by an stimulus of the opposite polarity. We will explore here the main dynamics properties of current-controlled memristors (CCM) where Z= I in Eq. (2).

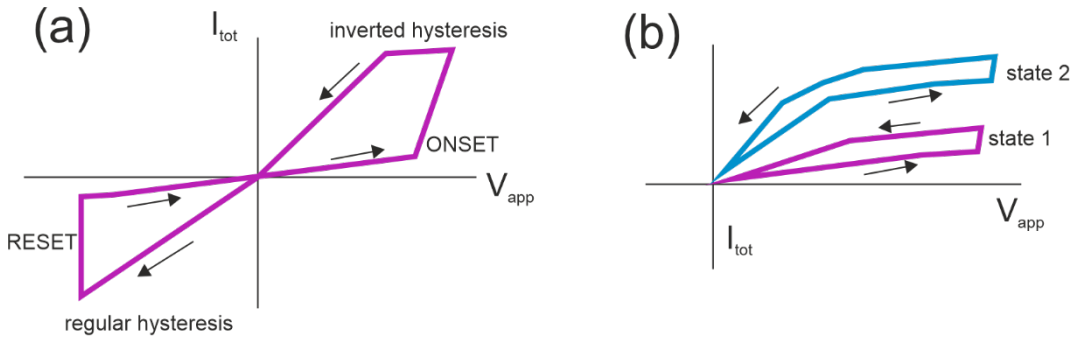

Fig. 1. (a) The onset of the memristor from a low resistance state to a high resistance state at positive voltage requires inverted (counterclockwise, inductive) hysteresis. The reset to the low resistance state in the negative polarity shows regular (clockwise,

capacitive) hysteresis. (b) Successive application of voltage sweep cycles increases the conduction state causing potentiation of the synapse, by reaching states of higher conductivity.

Memristors defined as in (1-2) constitute a broad family of models with varied physical interpretations, such as the celebrated Hogdkin-Huxley model of biological neurons [8-12], and metal-oxide switching devices [13-15]. Using the resistance switching capabilities of memristors, data can be stored and retained even when the power is turned off. This application can lead to faster and more energy-efficient storage solutions as an alternative to traditional non-volatile memory technologies like flash memory. Memristors can also perform analog computations by exploiting their resistance modulation characteristics [16-19]. This allows for the development of circuits that can process continuous signals in a more efficient and compact manner compared to traditional digital computation. In the application of a memristor as a synapse for neuromorphic computational systems, it must display distinct non-volatile resistive states that can support spike timing-dependent plasticity, as shown in Fig. 1b [20-32].

While the physical interpretation of memristors can be widely different, their main properties are (a) highly nonlinear characteristics in the functions F and g, and (b) significant memory effect which implies that the current value of Y depends on the history of the sample by the need to integrate the Eq. (2). The memory effect causes hysteresis in current-voltage curves, which has been the object of many recent discussions, for example in photovoltaic halide perovskites devices and memristors [33,34], where the hysteresis feature is generally attributed to the combination of ionic and electronic transport [35-38].

Hysteresis in photovoltaic cells is connected to the presence of negative capacitance [39,40]. A stabilized negative capacitance is an important goal for next generations of low consumption microelectronics. The role of the negative capacitor is to lower the power consumption in field-effect transistors, by reducing the subthreshold swing factor below the thermodynamic limit of 60 mV per decade. Recently there has been an extensive investigation of ferroelectrics with negative capacitance [41-43]. But the origin of negative capacitance in ferroelectric capacitors or ferroelectric-based superlattices remains unclear, being considered either a transitory product of polarization switching or an intrinsic phenomenon related to the presence of ferroelectric polarization [44]. Negative capacitances in electrochemical systems were reported over many years [45]. However, basic models indicate that "equilibrium" states that result in predictions of $C < 0$ are inherently unstable, representing local peaks in the thermodynamic potential. Consequently, predictions of $C < 0$ in open systems must be evaluated for stability and the presence of alternative, locally stable states [46].

Here we address the connection of the structural equations (1-2) to a negative capacitance effect in current-controlled memristors. In general, developing a system of

differential equations into a linear approximation at a specific stationary point is a valuable resource for gaining a deeper comprehension of a nonlinear system [47]. By keeping only linear terms one can obtain a diagnosis of the stability without solving the full nonlinear system [48]. The experimental method to measure a small perturbation over a steady state at different frequencies forms the basis of impedance spectroscopy, a technique utilized in various fields [49-51]. The method serves as a potent tool in electrical engineering for establishing connections between nonlinear models and linear data [52,53]. We will employ the method of small ac perturbation to derive equivalent circuits that inform us about stability, hysteresis, and other dynamical characteristics [10,12,54,55].

In section 2 we introduce the typical model of current-controlled memristors, and in section 3 we develop a general analysis of impedance, equivalent circuit, and stability of the dynamical systems. In Section 4 we comment on main properties of hysteresis of current-voltage curves. Thereafter we analyze these properties in several relevant examples, first a linear model system (section 5) and then some physical models that have been discussed in different fields: the discharge tube (section 6) and the titanium dioxide memristor (section 7). We finish with a list of experimental recommendations and some conclusions.

2. General memristor models in conducting devices

The memristor can be controlled either by voltage or current, according to the forcing variable in Eq. (2). For the current I_{tot} with respect to voltage u in a semiconductor device, a voltage-controlled memristor based on the general expressions (1-2) takes the form[5]

$$I_{tot} = C_m \frac{du}{dt} + f(u,x) \tag{3}$$

$$\tau_k \frac{dx}{dt} = g(u,x) \tag{4}$$

Here f is a conductivity function. In Eq. (3) we have also included the capacitive charging term of the geometric or contact capacitance $C_m > 0$ that is present in electronic devices.

There are many examples of applications of voltage-controlled memristors.[8-15] In fact most biological systems contain voltage-controlled memristors since the ion channels of cells are voltage-gated [56,57] which produces the dominant trend for artificial neurons and synapses in neuromorphic computation [58]. It has been generally shown that Eqs. (3-4) produce equivalent circuit structure of a chemical inductor, indicated in Fig. 2a [11]. Therefore voltage-controlled memristors produce an inductive effect, as it has been observed in many instances in semiconductor devices [59-62].

The complementary possibility to Eq. (4) is a CCM defined by Eq. (3) and

$$\tau_k \frac{dx}{dt} = h(I_{tot},x) \tag{5}$$

In comparison to the voltage controlled memristors, the CCM have been relatively

less exploited [4,5,63-65]. Some ac impedance properties of CCM were described by Chua and Sung [5,66]. The remaining of this work will focus on the two-dimensional dynamical system of the CCM (containing a single state variable).

It should be remarked that Eqs. (3 , 5) form a minimal model containing the main characteristics of memristors. In practice a device model can become much more complicated, including internal voltages such as at grain boundaries, additional derivatives due to charge storage at traps and interfaces, and a larger set of state variables that can produce additional dynamical features [67-73]. Nevertheless the simple CCM of Eqs. (3, 5) provides important insights about essential memristive properties that will be obtained in the context of larger or extended models.

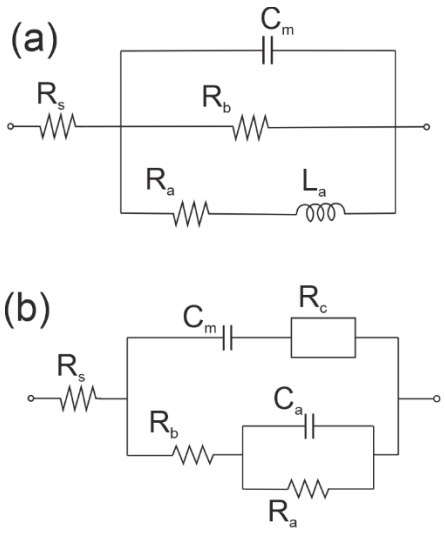

Fig. 2. Equivalent circuit representation of the impedance of chemical inductor (a) and current-controlled memristor (b). The square resistance is $R_c = -R_b C_m C_a \omega^2$.

3. Impedance and stability

To obtain insight to the properties of the dynamical system (3, 5) we consider the small signal expansion, where small perturbation quantities are denoted $\hat{y}$. The ac impedance is the voltage-to-current relationship at a frequency ω [10,12]. The small signal perturbation and Laplace transform $d/dt \to s$, where $s = i\omega$, give the equations

$$\hat{I}_{tot} = C_m s\hat{u} + f_u\hat{u} + f_x\hat{x} \tag{6}$$

$$\tau_k s\hat{x} = h_x\hat{x} + h_I\hat{I}_{tot} \tag{7}$$

The impedance has the form

$$Z(s) = \frac{\hat{u}}{\hat{I}_{tot}} = \frac{1}{1+R_b C_m s}\left(R_b + \frac{1}{\frac{1}{R_a}+sC_a}\right) \tag{8}$$

where the circuit elements are defined as follows:

$$R_b = \frac{1}{f_u} \tag{9}$$

$$R_a = \frac{f_x h_I}{f_u h_x} \tag{10}$$

$$C_a = -\frac{f_u}{f_x h_I}\tau_k \tag{11}$$

We introduce the time constants

$$\tau_m = R_b C_m \tag{12}$$

$$\tau_a = R_a C_a = -\frac{\tau_k}{h_x} \tag{13}$$

We consider that x is a slow variable provided that $\tau_a \gg \tau_m$ [10].

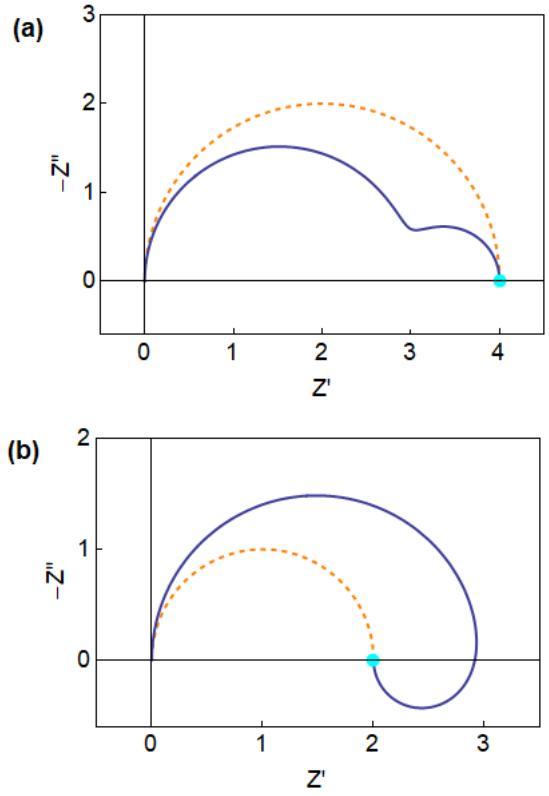

Fig. 3. Impedance spectra of the model memristor for parameters $C_m = 0.1$, $R_b = 3$, with two cases (a) $R_a = 1, C_a = 10$, (b) $R_a = -1, C_a = -10$. The cyan point is the resistance at zero frequency R_{dc} and the dashed line arc is the parallel combination $R_{dc}C_m$.

The equivalent circuit corresponding to Eq. (8) is shown in Fig. 2b and typical spectra in Fig. 3. The dc resistance is

$$R_{dc} = R_a + R_b \tag{14}$$

In previous results on this topic [5,11,74] it was commented that the CCM produces no inductor but a parallel $R_a C_a$ connection. Fig. 2 shows again this feature but extends

the previous results by including the capacitance C_m. We remark that elements of the equivalent circuit R_a, C_a, R_c can be positive or negative. In particular Fig. 2b can contain a capacitive element with a negative sign, $C_a < 0$, i.e. a truly negative capacitance.

In Eq. (3) we added the passive capacitor C_m by physical reasons, but we note that it leads to a two-dimensional dynamical system capable of complex behaviour as self-sustained oscillations [10,12]. The $R_b < 0$ (giving $\tau_m < 0$) is a well-known cause of instability and oscillatory behaviour, as in the FitzHugh-Nagumo neuron model [75]. Let us assume $R_b > 0$ to focus on the properties that are specific to the CCM.

We observe in Fig. 2b that the model produces a negative frequency-dependent resistor given by

$$R_c = -R_b C_m C_a \omega^2 \tag{15}$$

The negative elements in the equivalent circuit are often a cause of instability and self-sustained oscillatory behaviour related to Hopf bifurcations [10,12]. In fact the element R_c in Eq. (15) has been shown to produce a dynamical instability [76]. For a general analysis of the stability of the system (3, 5) we calculate the Jacobi matrix of Eqs. (6-7). We obtain the determinant

$$\Delta = \begin{vmatrix} -\frac{f_u}{C_m} & -\frac{f_x}{C_m} \\ 0 & \frac{h_x}{\tau_k} \end{vmatrix} = -\frac{f_u h_x}{C_m \tau_k} = \frac{1}{\tau_m \tau_a} \tag{16}$$

and the trace of the matrix is

$$T_\lambda = -\frac{1}{\tau_m} - \frac{1}{\tau_a} \tag{17}$$

Instability occurs if $\Delta < 0$ or $T_\lambda > 0$ leading to different classes of behaviours [47,77-79]. Since we assumed that $\tau_m < 0$, the system is stable provided that $\tau_a > 0$, hence the condition for stability is $h_x < 0$, composed of the cases 1-4 of Table 1.

The fixed point becomes an unstable source and generates a limit cycle trajectory when $\Delta > 0$ and $T_\lambda > 0$, with the Hopf bifurcation occurring at $T_\lambda = 0$. But such conditions cannot coexist in our system, even if $R_b < 0$. The oscillatory behaviour involving the dynamic negative resistance has been obtained in a more complex voltage-controlled three-dimensional system (with two state variables) [76]. On the other hand the current system allows stable situations $\Delta > 0$ in which the dc resistance $R_{dc} < 0$, as previously found for negative inductors [10].

In summary the simple two-dimensional CCM produces a positive or negative capacitance when it is stable, but not self-sustained oscillations.

Table 1. Sign of the equivalent circuit elements (> or < 0) of the current-controlled memristor.

	R_b	h_x	f_x	h_I	R_a	C_a	R_c	τ_a
1	+	-	+	+	-	-	-	+
2	+	-	+	-	+	+	+	+
3	+	-	-	+	+	+	+	+

4	+	-	-	-	-	-	-	+
5	+	+	+	+	+	-	-	-
6	+	+	+	-	-	+	+	-
7	+	+	-	+	-	+	+	-
8	+	+	-	-	+	-	-	-

4. Hysteresis

The types of hysteresis in current-voltage curves and their physical interpretation have been recently discussed [68,70,80], as mentioned above. The hysteresis loop can be clockwise in "regular hysteresis", or counterclockwise in "inverted hysteresis". Fig. 1a summarizes the situation for a bipolar switching device, in which the *set* operation takes place on one polarity of the voltage or current, and the *reset* operation requires the opposite polarity [1]. We observe that the set cycle produces an inverted hysteresis loop. This is characterized by a forward current that is smaller than the reverse current, and it is associated to the inductive characteristic in Fig. 2a [39,40,68]. Note that the chemical inductor is not a "parasitic element" [72], it is rather the intrinsic fingerprint of the memristor device [11].

On the other hand in the reset operation the current at reverse bias is higher than in the forward direction, as corresponds to a (positive) capacitive element. Determining the current at increasing scan rates is the standard method of measurement of capacitance in electrochemistry [81].

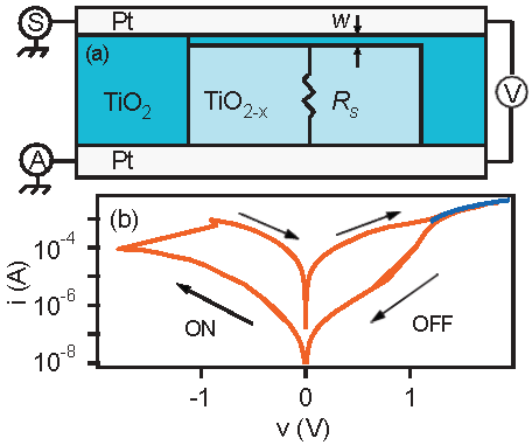

Fig. 4. (a) Schematic of the TiO_2 memristor device and the four-wire time-sampled current-voltage test setup used for the state-test protocol. w and R_s represent the tunneling barrier width and the electroformed channel resistance, respectively. (b) Example switching $I-V$ curve. Positive polarity turns the device state to off, while negative polarity turns the device on. The blue curve corresponds to the fit for a conducting channel series resistance of R_s = 215 ± 6 D. Reproduced with permission

from [82]. Pickett, M. D.; Strukov, D. B.; Borghetti, J. L.; Yang, J. J.; Snider, G. S.; Stewart, D. R.; Williams, R. S. Switching dynamics in titanium dioxide memristive devices, *J. Appl. Phys.* **2009**, *106*, 074508. Copyright 2009 American Phsyical Society.

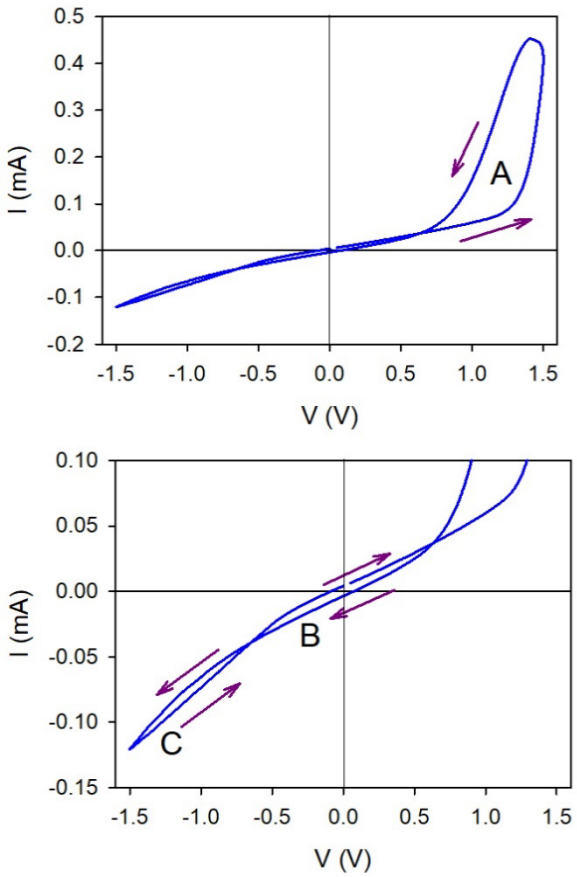

Fig. 5. Current-voltage characteristic for a FTO/PEDOT:PSS/ $MAPbI_3$/Spiro-MeOTAD /Au memristor device at scan velocity 0.5 V/s. Reproduced with permission from [83], Berruet, M.; Pérez-Martínez, J. C.; Romero, B.; Gonzales, C.; Al-Mayouf, A. M.; Guerrero, A.; Bisquert, J. Physical model for the current-voltage hysteresis and impedance of halide perovskite memristors, *ACS Energy Lett.* **2022**, *7*, 1214–1222; licensed under a Creative Commons Attribution (CC BY 4.0) license.

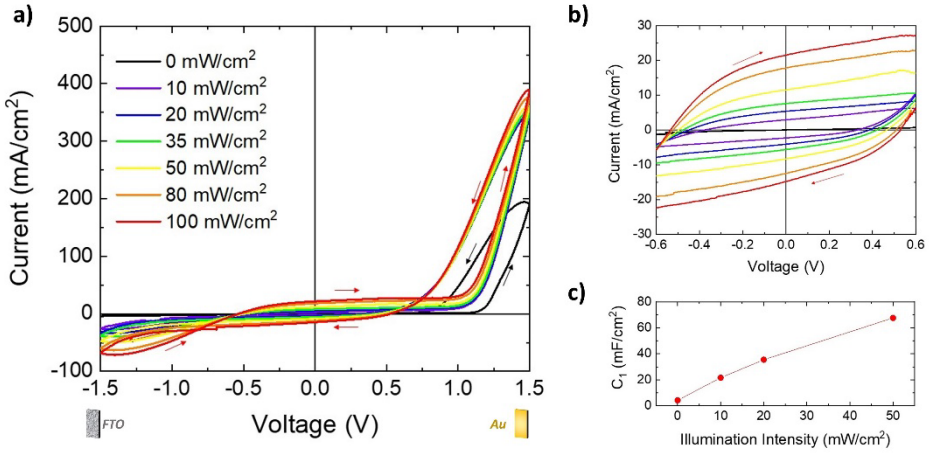

Fig 6. a) Current density -voltage characteristic of a FTO/PEDOT:PSS/$MAPbI_3$/Au memristor measured from 0 to 100 mW/cm^2 using a blue light source (470 nm) and 0.1 cm^2 active area. Panel b) corresponds to a magnified view of the scale. c) Low frequency capacitance enhancement with illumination intensity. Reproduced with permission from [84]. Munoz-Diaz, L.; Rosa, A. J.; Bou, A.; Sanchez, R. S.; Romero, B.; John, R. A.; Kovalenko, M. V.; Guerrero, A.; Bisquert, J. Inductive and Capacitive Hysteresis of Halide Perovskite Solar Cells and Memristors Under Illumination, *Frontiers in Energy Research* **2022**, *10*, 914115.; licensed under a Creative Commons Attribution (CC BY 4.0) license.

From Fig. 1a we conclude that semiconductor memristors display a large *inverted* hysteresis loop in the set cycle, where the current raises at a certain threshold of voltage or current [68,70,80]. In Fig. 1a the set cycle is at positive voltage, but Fig. 4 shows and example [82] where the switch to high current occurs at negative polarity with inverted hysteresis. In general current-voltage curve can be self crossing, as in Fig. 1a, or not [7,66]. If it is self crossing then the hysteresis changes from inverted in the set region to regular in the reset polarity, as in the case of Fig. 4.

The current-voltage curves can become more complex according to the internal dynamics of the memristor as represented by additional equivalent circuit elements [66,72]. Fig. 5 shows the hysteresis properties of a methylammonium lead iodide perovskite memristor [83] in which there are two crossings: The region A is a large inverted hysteresis loop due to the set cycle. Then B is a capacitive region and the next crossing causes yet another inductive loop at the reset voltage. We note that the capacitive property around the origin is related to the capacitance introduced in Eq. (3), whereby the current-voltage curve cannot pass through the origin, a feature that is found in different types of systems [85]. In Fig. 6 we show similar results for another memristor [84], but under different levels of illumination. We observe that the capacitive loop around the origin becomes more pronounced at higher light intensity,

Fig. 6b. This is due to the property of the large increase of the capacitance of halide perovskites with illumination [49,86], that is shown in Fig. 6c.

The changes of hysteresis from capacitive to inductive indicate a transition of the dominant properties of the equivalent circuit according to the ranges of applied voltage or current [68]. The analysis of these features requires more complex models than the basic one shown in Eqs. (3, 5) [67].

5. Minimal model of the current-controlled memristor

In order to explore basic dynamical properties of CCMs we present a simple linear model as follows

$$I_{tot} = \frac{u}{R_b} + c\, w + C_m \frac{du}{dt} \tag{18}$$

$$\tau_k \frac{dw}{dt} = a I_{tot} - \frac{w}{b} \tag{19}$$

Here w is a slow current variable and a, b, c, R_b are constants. The dc current is

$$I_{dc} = \frac{1}{1-abc}\frac{u}{R_b} \tag{20}$$

We obtain the derivatives $f_w = c$, $h_I = a$, $h_w = -1/a$, hence

$$R_a = -abcR_b \tag{21}$$

$$C_a = -\frac{\tau_k}{acR_b} \tag{22}$$

$$\tau_a = R_a C_a = b\tau_k \tag{23}$$

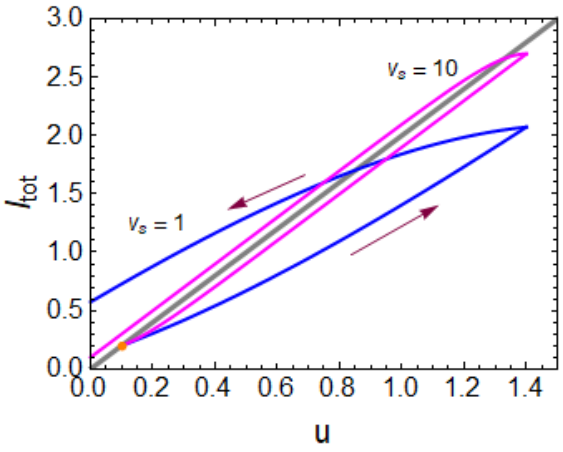

Fig. 7. Current-voltage curves at constant voltage sweep of velocity v_s, starting at the equilibrium $I_{ss}(u_0)$ (grey line, orange point), from $u_0 = 0.1$ to $u_1 = 1.4$. Parameters $d = 0.5, V_T = 0.5; I_s = 1; a = 1, b = 1, \tau_k = 0.01, R_b = 0.5, R_s = 0, C_m = 0$.

Let us assume that $a, b, c > 0$ and $abc < 1$. Then the model generates a negative R_a and negative C_a quite naturally. The linear sweep voltammetry where the voltage $u = v_s t$ at sweep rate v_s is shown in Fig. 7. We observe that hysteresis is inverted, just as it

occurs with the systems dominated by the chemical inductor in Fig. 1a [68]. In fact it is plausible that the inductor and the negative capacitor produce the same type of effect, since a larger sweep velocity produces a decreasing current for them both, in contrast to the positive capacitor (in which current increases with scan rate). The role of the negative R_a is to equilibrate the negative capacitance response by the resulting positive τ_a, as mentioned before.

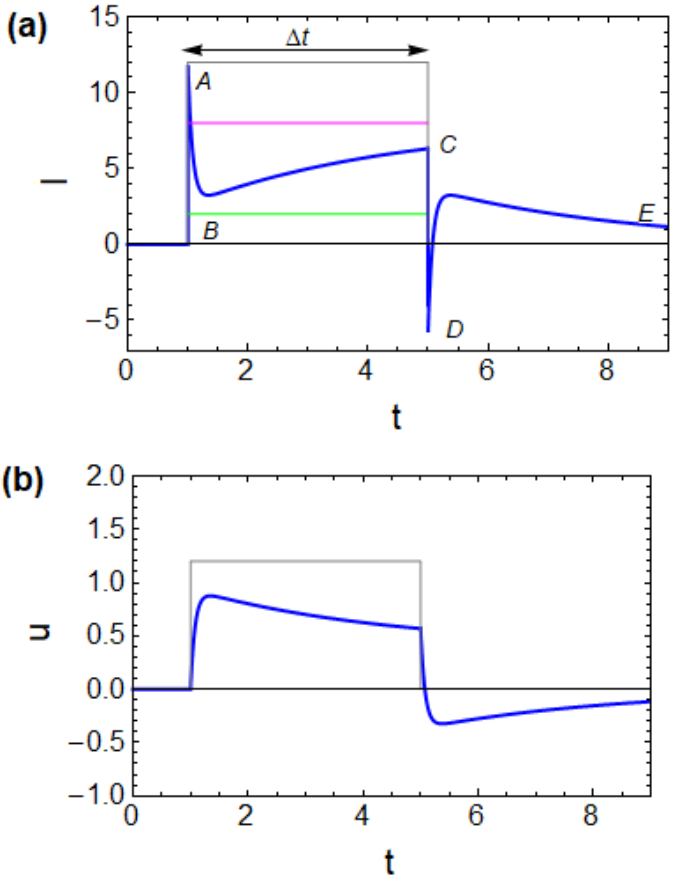

Fig. 8. (a) Transient charging current for the linear memristor model for a square voltage pulse $V_{app} = 1.5$ of duration Δt. Parameters . Parameters $d = 0.5, V_T = 0.5; I_s = 1; a = 1, b = 1, \tau_k = 0.01, R_b = 0.5, R_s = 0.1, C_m = 1$. Grey line is $\Delta I = V_{app}/R_s$, green line is $V_{app}/(R_s + R_b)$, and purple line is $I_{dc}(V_{app})$. (b) Evolution of the internal voltage. The grey line is V_{app}.

Another important dynamical feature is the current in response to a voltage pulse of magnitude V_{app} and duration Δt, indicated in grey lines in Fig. 8. For this measurement we consider the effect of the series resistance R_s as in Fig. 2b, takes a voltage drop $I_{tot}R_s$ as follows

$$V_{app} = R_s I_{tot} + u \tag{24}$$

We solve (18), (19) and (24) for the square voltage perturbation and the result is shown in Fig. 8a. The response of the CCM with negative capacitance is similar to that of the voltage controlled memristor that has been described recently [54]. These features can be understood by reference to the equivalent circuit 2b. In the first instant (A) the capacitor C_m does not have charge and all the applied voltage drops at the series resistance. Thereafter the positive capacitor C_m charges over the characteristic time $\tau_s = R_s C_m$. The negative capacitor C_a has no charge yet due to the longer time constant τ_a. Hence the current goes to the lowest point (B) until the C_a starts charging and then raises again, since the associated resistance R_a is negative and the overall resistance decreases.

The rise of the current, which in voltage-controlled memristors is due to the intrinsic chemical inductor as shown before [55], is the essential property of the potentiation of artificial synapses, in which the conductivity increases by external impulses [25-32] as shown in Fig. 1b. These transient behaviour properties are well known in biological neural systems [87]. Fig. 8a shows that the *same effect* can be obtained by the negative capacitance and negative resistance that are intrinsic properties to the CCM.

Continuing the description of the response to the pulse, after stage B the current aims to reach the stationary value given by the purple line. However if the negative capacitance time $\tau_a > \Delta t$ the current does not reach the maximum possible value at the point C. The next feature is the inverted peak when the voltage is disconnected, D [88]. This is due to the inversion of the voltage in the series resistance to cancel the remaining u, that is shown in Fig. 8b. We observe that the internal voltage maintains a negative value in the disconnected pulse time Δt, that will cause a larger response in the next voltage step, producing the potentiation effect [55].

The previous discussion uses a simple linear model of Eqs. (18-19). Normally memristors show highly nonlinear properties, but the linearized equations that give the impedance spectra and stability properties will be qualitatively similar in most cases, according to the general theory of dynamical systems [47]. For example let us consider a more realistic current form of exponential dependence on voltage [13,15,65,82] related to the Simmons tunneling model [89].

$$I_{tot} = I_s^{1-d} w^d e^{u/V_T} \tag{25}$$

where d is a constant, and Eq. (25) is combined with Eq. (19). In the steady state

$$I_{ss}(u) = I_s (ab)^{\frac{d}{1-d}} e^{u/(1-d)V_T} \tag{26}$$

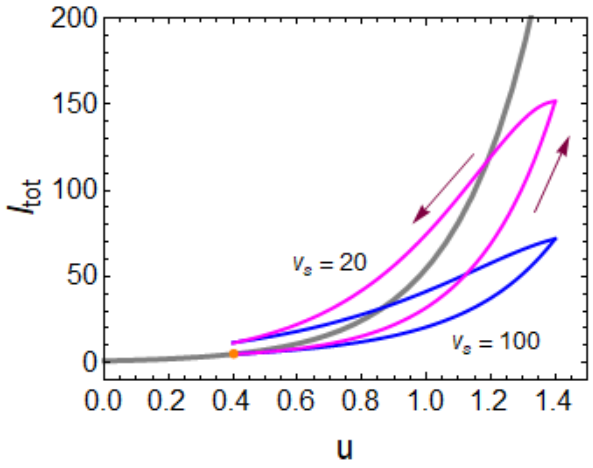

Fig. 9. Current-voltage curves at constant voltage sweep of velocity v_s, starting at the equilibrium $I_{ss}(u_0)$ (grey line, orange point), from $u_0 = 0.4$ to $u_1 = 1.4$. Parameters $d = 0.5, V_T = 0.5; I_s = 1; a = 1, b = 1, \tau_k = 0.01, R_s = 0, C_m = 0$.

The resulting current-voltage curves are shown in Fig. 9, and again we obtain the inverted hysteresis property, since the signs of the equivalent circuit elements are the same as in Fig. 7 (negative C_a and negative R_a).

6. The discharge tube

The following model was used by Francis [90] to describe the behaviour of discharge tubes

$$I_{tot} = \frac{xu}{k} \tag{27}$$

$$\frac{dx}{dt} = \alpha I_{tot} u - \beta x \tag{28}$$

Here x is the electron density in the tubes and α, β, k are constants. Note that the equilibrium voltage is given by the unique value $u_1 = (k\beta/\alpha)^{1/2}$ and the current reaches any equilibrium value $I_{app} = (\beta/\alpha k)^{1/2} x_1$ according to the internal value x_1. Chua and Sung [5] wrote Eq. (28) as

$$\frac{dx}{dt} = \frac{\alpha k}{x} I_{tot}^2 - \beta x \tag{29}$$

and they present the model as an example of CCM [66].

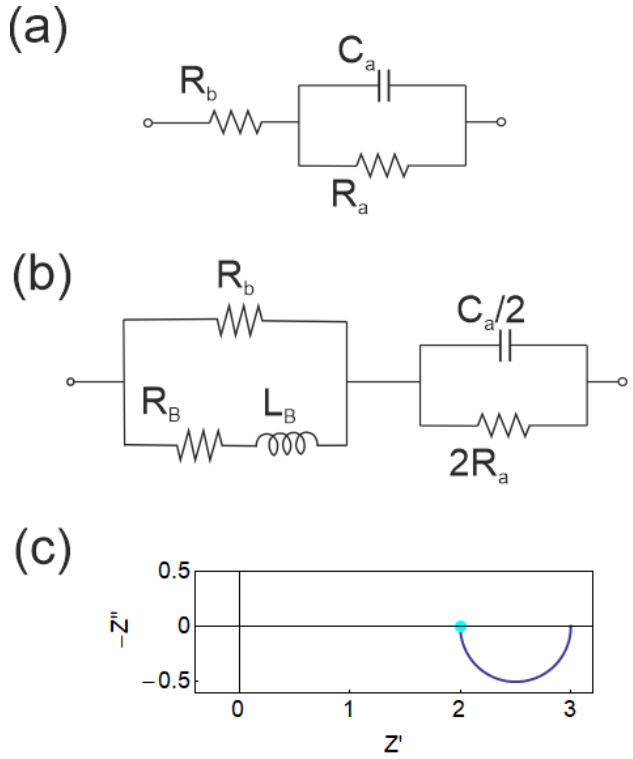

Fig. 10. Equivalent circuit of (a) current-controlled memristor and (b) a mixed voltage and current control memristor model. (c) Impedance spectrum with $C_m = 0, R_b = 3, R_a = -1, C_a = -10$.

If we apply (9-11) to the model (27, 29) we obtain the equivalent circuit of Fig. 10a, that corresponds to Fig. 2a with $C_m = 0$. The circuit parameters are

$$R_b = \frac{k}{x} \tag{30}$$

$$R_a = -\frac{1}{\frac{x}{2k} + \frac{\beta x}{2\alpha u^2}} \tag{31}$$

$$C_a = -\frac{x}{2\alpha u^2} \tag{32}$$

Clearly the model generates directly negative resistance R_a and capacitance C_a with the resulting spectrum in Fig. 10c. Since $h_x = -\beta < 0$, the model is stable, with the time constant

$$\tau_a = R_a C_a = \frac{1}{\beta + \frac{\alpha u^2}{k}} \tag{33}$$

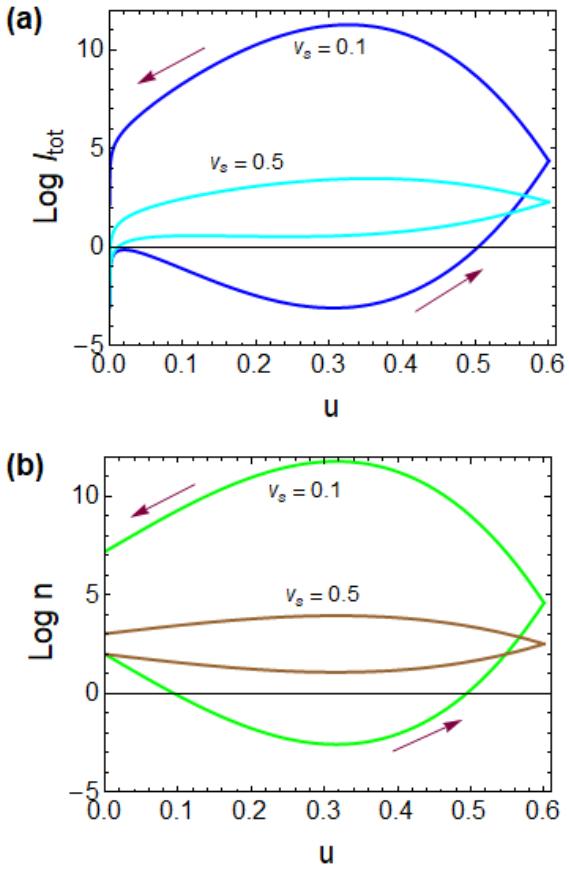

Fig. 11. (a) Current-voltage curves and (b) carrier density at constant voltage sweep of velocity v_s. Parameters $\alpha = 50, k = 1, \beta = 5, x_0 = 100$.

The current-voltage curves at constant voltage sweep rate are shown in Fig. 11a, associated to the changes of electron density in Fig. 11b. It is clear that a large inverted hysteresis is observed, due to the negative capacitance effect.[68,84] Furthermore the full diagram is not self-crossing at the origin so that inverted hysteresis occurs at both polarities [66].

The definition of the current controlled memristor in Eq. (29) is not sharp. In fact one can easily exchange the current or voltage control property as desired, applying Eq. (27). If we calculate the impedance using Eq. (28) we obtain the equivalent circuit in Fig. 11b where

$$R_B = \frac{\beta k^2}{\alpha x u^2} \tag{34}$$

$$L_B = \frac{k^2}{\alpha x u^2} \tag{35}$$

Both circuits in Fig. 10a and 10b are fully equivalent. We see that the Fig. 10a has been split in two identical halves in Fig. 10b and one of them has been transformed to an inductive circuit using the transformation presented by Klotz [91]. This is a general

feature of impedance models, associated to the possibility of the transformation of internal variables [92]. We remark, however, that the presence of the geometrical capacitance in Eq. (3) removes the freedom to convert between voltage- and current-controlled memristors. Therefore, the configuration depicted in Figure 2b is more challenging to modify, and the components take on a tangible meaning.

7. The titanium-dioxide memristor

We analyze the titanium-dioxide film that was the first device claimed to be a memristor [4,93]. The memristive property is the variation of dopants concentration in the semiconductor film that switches between low (off) and high (on) conduction states. The doped region thickness is x that satisfies $x_{off} < x < x_{on}$, with a total thickness $D = x_{off} - x_{on}$. The model is defined by the following equations including materials constants R_{on}, R_{off}, μ ;

$$I_{tot} = \frac{u}{R_0(x)} \tag{36}$$

$$R_0(x) = R_{on} + \frac{\Delta R}{D}(x - x_{on}) \tag{37}$$

$$\frac{dx}{dt} = \mu \frac{R_{on}}{D} I_{tot} \tag{38}$$

Here $\Delta R = R_{off} - R_{on}$. The partial derivatives have the expressions

$$f_u = \frac{1}{R_0(x)} \tag{39}$$

$$f_x = -\frac{1}{R_0(x)^2} \frac{\Delta R}{D} u \tag{40}$$

$$h_I = \mu \frac{R_{on}}{D} \tag{41}$$

$$h_x = 0 \tag{42}$$

The equivalent circuit elements are

$$R_b(x) = R_0(x) \tag{43}$$

$$C_a(x) = \frac{R_0(x)}{R_{on}\Delta R} \frac{D^2}{\mu u} \tag{44}$$

We also obtain $R_a = \infty$, owing to the strange result $h_x = 0$. It implies that in Fig. 2c, R_a is an open circuit element, so that the device has no dc conduction channel. In fact in Eq. (38) there is no x dependence, and the only solution is steady state is $I_{tot} = 0$. This is not in agreement with the fact that the model has an intrinsic large resistance R_{off}. The problem of a vanishing current-voltage curve is inherent to the original definition of memristor [94].

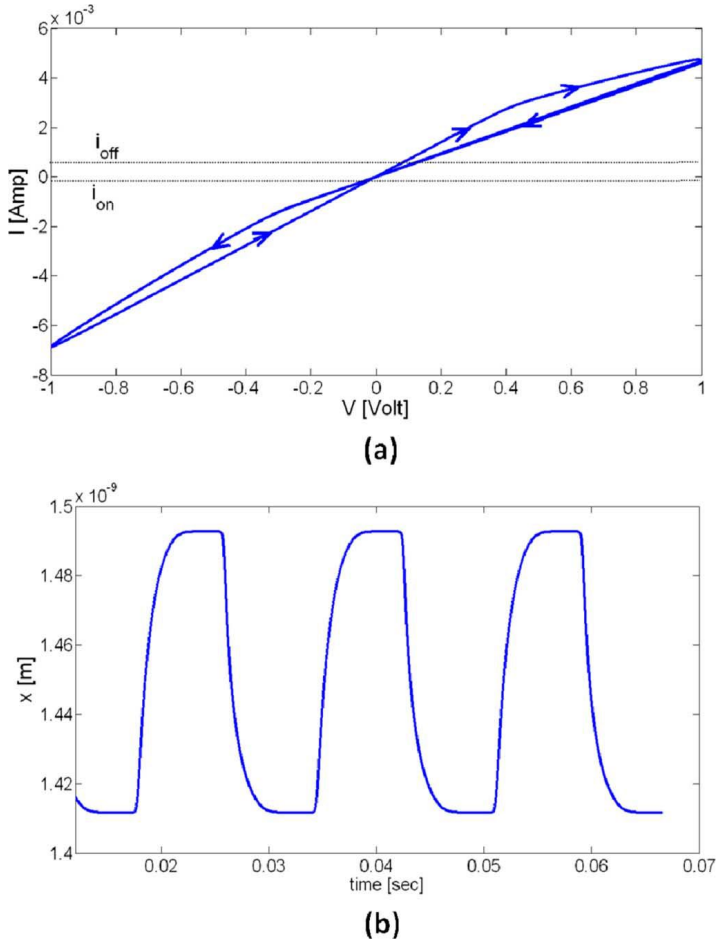

Fig. 12. The TEAM memristor model driven with a sinusoidal input of 1 volt. (a) I-V curve, $R_{ON} = 50\ \Omega, R_{OFF} = 1\ k\Omega$, and (b) state variable x. Reproduced with permission from[65] Kvatinsky, S.; Friedman, E. G.; Kolodny, A.; Weiser, U. C. TEAM: ThrEshold Adaptive Memristor Model, *IEEE Transactions on Circuits and Systems I: Regular Papers* **2013**, *60*, 211-221. Copyright 2013 IEEE.

To solve this problem, a better definition of memristive systems incorporating the slow state variables was later introduced, according to Eqs. (1-2) [5]. The model of Eq. (38-40) has also been completed in this fashion [82], so that it has a stationary-current-voltage characteristic, and different version have been developed to explain the dynamic characteristics. One model suggested in the literature has the following equations [65] for the current (i) controlled slow variable x of the Eq. (38)

$$\frac{dx}{dt} = k_{off}\left(\frac{i(t)}{i_{off}} - 1\right)^{\alpha_{off}} exp\left[-exp\left(\frac{x-a_{off}}{w_c}\right)\right], 0 < i_{off} < i \quad (45)$$

$$\frac{dx}{dt} = 0\ , i_{on} < i < i_{off} \quad (46)$$

$$\frac{dx}{dt} = -k_{on}\left(\frac{i(t)}{i_{on}} - 1\right)^{\alpha_{on}} exp\left[-exp\left(-\frac{x-a_{on}}{w_c}\right)\right], i < i_{on} < 0 \quad (47)$$

A number of kinetic constants have been introduced. The exponential terms have the

role to confine the variable x in the segment (a_{off}, a_{on}).

Applying the method of Section 3 to calculate impedance parameters, we find the results in Table 2. Therefore we obtain that both current regions for *on* ($i < i_{on}$) and off ($i_{off} < i$) states are stable. But the signs of the capacitances are opposite in them. The *on* region has a negative capacitance, while the *off* region has positive capacitance. Correspondingly, the first region shows inductive hysteresis and the second region shows capacitive hysteresis. This is the case as shown in Fig. 12a. Consequently the impedance structure of the model is able to predict the dominant dynamical characteristics.

Table 2. Sign of impedance components of model (45-47).

	f_u	f_x	h_I	h_x	R_a	C_a	τ_a
$0 < i_{off} < i$	-	-	+	-	+	+	+
$i < i_{on} < 0$	+	-	-	-	-	-	+

8. Experimental protocol

To summarize the analysis explained in this paper, we suggest that the study of a new system should contain the following complementary measurements.

a) Establish the steady state current-voltage curve (at very slow measurement speed).
b) Measure the current voltage curves at different voltage sweep rates. This procedure can identify the dominant sectors of regular and inverted hysteresis and their combinations.
c) Measure the impedance spectroscopy response at different points of the stationary current-voltage curve.
d) Measure the transient decay for a perturbation of current or voltage at different points of the stationary current-voltage curve.

As we have remarked, (c) provides the elements of the equivalent circuit that determine the local properties of hysteresis and enables an interpretation of the large voltage excursions of (b). However, the impedance measurement is very long if the low frequencies are probed. It may be difficult to perform in the region of the I-V plane close to the resistive switching, where a steady state cannot be stabilized [95]. Therefore the measurement (d) can be used as it reveals the dominant elements of the equivalent circuit in a faster measurement.

Conclusion

The general analysis of impedance properties of the current-controlled memristors shows that equivalent circuit elements of different signs emerge depending on the derivatives of the dynamical equations. We obtained the criteria for stability, and we

showed that the negative capacitance emerges very easily in the current-controlled memristors. When it is combined with a negative resistance, the system is stable, and produces inverted (inductive) hysteresis in the onset of the low resistance state of the memristor. The method is applied to several devices obtained in the literature, and we showed that it is quite useful for obtaining insight of the dynamical behaviour of these highly nonlinear systems.

Acknowledgements

We thank MICINN for support by the project EUR2022-134045.

Data availability statement

Data sharing not applicable – no new data generated

References

[1] R. Waser and M. Aono, Nanoionics-based resistive switching memories, Nat. Mater. **6**, 833 (2007).

[2] M. D. Ventra, Y. V. Pershin, and L. O. Chua, Circuit Elements With Memory: Memristors, Memcapacitors, and Meminductors, Proceedings of the IEEE **97**, 1717 (2009).

[3] T. Prodromakis, C. Toumazou, and L. Chua, Two centuries of memristors, Nat. Mater. **11**, 478 (2012).

[4] D. B. Strukov, G. S. Snider, D. R. Stewart, and R. S. Williams, The missing memristor found, Nature **453**, 80 (2008).

[5] L. O. Chua and K. Sung Mo, Memristive devices and systems, Proceedings of the IEEE **64**, 209 (1976).

[6] L. Chua, Resistance switching memories are memristors, Appl. Phys. A **102**, 765 (2011).

[7] Y. V. Pershin and M. Di Ventra, Memory effects in complex materials and nanoscale systems, Adv. Phys. **60**, 145 (2011).

[8] A. L. Hodgkin and A. F. Huxley, A quantitative description of membrane current and its application to conduction and excitation in nerve, J Physiol **117**, 500 (1952).

[9] L. Chua, V. Sbitnev, and H. Kim, Hodgkin–Huxley axon is made of memristors, International Journal of Bifurcation and Chaos **22**, 1230011 (2012).

[10] J. Bisquert, Negative inductor effects in nonlinear two-dimensional systems. Oscillatory neurons and memristors, Chemical Physics Reviews **3**, 041305 (2022).

[11] J. Bisquert and A. Guerrero, Chemical Inductor, J. Am. Chem. Soc. **144**, 5996 (2022).

[12] J. Bisquert, Hopf bifurcations in electrochemical, neuronal, and semiconductor

systems analysis by impedance spectroscopy, Appl. Phys. Rev. **9**, 011318 (2022).

[13] T. Chang, S.-H. Jo, K.-H. Kim, P. Sheridan, S. Gaba, and W. Lu, Synaptic behaviors and modeling of a metal oxide memristive device, Appl. Phys. A **102**, 857 (2011).

[14] D. P. Pattnaik, Y. Ushakov, Z. Zhou, P. Borisov, M. D. Cropper, U. W. Wijayantha, A. G. Balanov, and S. E. Savel′ev, Temperature Control of Diffusive Memristor Hysteresis and Artificial Neuron Spiking, Phys. Rev. Appl. **19**, 024065 (2023).

[15] L. Chen, C. Li, T. Huang, Y. Chen, S. Wen, and J. Qi, A synapse memristor model with forgetting effect, Physics Letters A **377**, 3260 (2013).

[16] D. V. Christensen, R. Dittmann, B. Linares-Barranco, A. Sebastian, and M. Le Gallo, 2022 roadmap on neuromorphic computing and engineering, Neuromorphic Computing and Engineering, DOI: 10.1088/2634 (2022).

[17] J. J. Yang, D. B. Strukov, and D. R. Stewart, Memristive devices for computing, Nature Nanotechnology **8**, 13 (2013).

[18] Y. Zhang *et al.*, Brain-inspired computing with memristors: Challenges in devices, circuits, and systems, Appl. Phys. Rev. **7**, 011308 (2020).

[19] J. Zhu, T. Zhang, Y. Yang, and R. Huang, A comprehensive review on emerging artificial neuromorphic devices, Appl. Phys. Rev. **7**, 011312 (2020).

[20] B. Linares-Barranco and T. Serrano-Gotarredona, Memristance can explain Spike-Time-Dependent-Plasticity in Neural Synapses, Nature Precedings, https://doi.org/10.1038/npre.2009.3010.1 (2009).

[21] S. H. Jo, T. Chang, I. Ebong, B. B. Bhadviya, P. Mazumder, and W. Lu, Nanoscale Memristor Device as Synapse in Neuromorphic Systems, Nano Lett. **10**, 1297 (2010).

[22] M. Prezioso, M. R. Mahmoodi, F. M. Bayat, H. Nili, H. Kim, A. Vincent, and D. B. Strukov, Spike-timing-dependent plasticity learning of coincidence detection with passively integrated memristive circuits, Nat. Commun. **9**, 5311 (2018).

[23] R. Kozma, R. E. Pino, and G. E. Pazienza, *Advances in Neuromorphic Memristor Science and Applications* (Springer, 2012).

[24] C. Wang *et al.*, Multi-State Memristors and Their Applications: An Overview, IEEE Journal on Emerging and Selected Topics in Circuits and Systems **12**, 723 (2022).

[25] W. Xu, H. Cho, Y.-H. Kim, Y.-T. Kim, C. Wolf, C.-G. Park, and T.-W. Lee, Organometal Halide Perovskite Artificial Synapses, Adv. Mater. **28**, 5916 (2016).

[26] J.-Q. Yang, R. Wang, Z.-P. Wang, Q.-Y. Ma, J.-Y. Mao, Y. Ren, X. Yang, Y. Zhou, and S.-T. Han, Leaky integrate-and-fire neurons based on perovskite memristor for spiking neural networks, Nano Energy **74**, 104828 (2020).

[27] X. Yang, Z. Xiong, Y. Chen, Y. Ren, L. Zhou, H. Li, Y. Zhou, F. Pan, and S.-T. Han, A self-powered artificial retina perception system for image preprocessing based on photovoltaic devices and memristive arrays, Nano Energy **78**, 105246 (2020).

[28] J. Gong, H. Wei, Y. Ni, S. Zhang, Y. Du, and W. Xu, Methylammonium halide-doped perovskite artificial synapse for light-assisted environmental perception and learning, Materials Today Physics **21**, 100540 (2021).

[29] S. Ham, S. Choi, H. Cho, S.-I. Na, and G. Wang, Photonic Organolead Halide Perovskite Artificial Synapse Capable of Accelerated Learning at Low Power Inspired by Dopamine-Facilitated Synaptic Activity, Adv. Func. Mater. **29**, 1806646 (2019).

[30] J. Lao *et al.*, An air-stable artificial synapse based on a lead-free double perovskite Cs2AgBiBr6 film for neuromorphic computing, J. Mat. Chem. C **9**, 5706 (2021).

[31] N. Ilyas, D. Li, C. Li, X. Jiang, Y. Jiang, and W. Li, Analog Switching and Artificial Synaptic Behavior of Ag/SiOx:Ag/TiOx/p++-Si Memristor Device, Nanoscale Research Letters **15**, 30 (2020).

[32] J. Ding, W. Gao, L. Gao, K. Lu, Y. Liu, J.-L. Sun, and Q. Yan, Unravelling the Effect of Halogen Ion Substitution on the Noise of Perovskite Single Crystal Photodetector, J. Phys. Chem. Lett. **13**, 7831 (2022).

[33] H.-S. Kim and N.-G. Park, Parameters Affecting I-V Hysteresis of CH3NH3PbI3 Perovskite Solar Cells: Effects of Perovskite Crystal Size and Mesoporous TiO2 Layer, J. Phys. Chem. Lett. **5**, 2927 (2014).

[34] H. J. Snaith *et al.*, Anomalous Hysteresis in Perovskite Solar Cells, J. Phys. Chem. Lett. **5**, 1511 (2014).

[35] E. Ghahremanirad, A. Bou, S. Olyaee, and J. Bisquert, Inductive Loop in the Impedance Response of Perovskite Solar Cells Explained by Surface Polarization Model, J. Phys. Chem. Lett., 1402 (2017).

[36] D. A. Jacobs, H. Shen, F. Pfeffer, J. Peng, T. P. White, F. J. Beck, and K. R. Catchpole, The two faces of capacitance: New interpretations for electrical impedance measurements of perovskite solar cells and their relation to hysteresis, J. Appl. Phys. **124**, 225702 (2018).

[37] F. Ebadi, N. Taghavinia, R. Mohammadpour, A. Hagfeldt, and W. Tress, Origin of apparent light-enhanced and negative capacitance in perovskite solar cells, Nat. Commun. **10**, 1574 (2019).

[38] D. Moia *et al.*, Ionic-to-electronic current amplification in hybrid perovskite solar cells: ionically gated transistor-interface circuit model explains hysteresis and impedance of mixed conducting devices, Energy Environ. Sci. **12**, 1296 (2019).

[39] A. O. Alvarez, R. Arcas, C. A. Aranda, L. Bethencourt, E. Mas-Marzá, M.

Saliba, and F. Fabregat-Santiago, Negative Capacitance and Inverted Hysteresis: Matching Features in Perovskite Solar Cells, J. Phys. Chem. Lett. **11**, 8417 (2020).

[40] J. Bisquert, A. Guerrero, and C. Gonzales, Theory of Hysteresis in Halide Perovskites by Integration of the Equivalent Circuit, ACS Phys. Chem Au **1**, 25 (2021).

[41] S. Salahuddin and S. Datta, Use of Negative Capacitance to Provide Voltage Amplification for Low Power Nanoscale Devices, Nano Lett. **8**, 405 (2008).

[42] J. Íñiguez, P. Zubko, I. Luk'yanchuk, and A. Cano, Ferroelectric negative capacitance, Nat. rev. Mater. **4**, 243 (2019).

[43] M. A. Alam, M. Si, and P. D. Ye, A critical review of recent progress on negative capacitance field-effect transistors, App. Phys. Lett. **114**, 090401 (2019).

[44] L. Pintilie, G. A. Boni, C. Chirila, L. Hrib, L. Trupina, L. D. Filip, and I. Pintilie, Polarization Switching and Negative Capacitance in Epitaxial PbZrO2Ti0.8O3 Thin Films, Phys. Rev. Appl. **14**, 014080 (2020).

[45] M. B. Partenskii and P. C. Jordan, The admissible sing of the differential capacity, instabilities, and phase transitions at electrified interfaces, J. Chem. Phys. **99**, 2992 (1993).

[46] M. B. Partenskii and P. C. Jordan, Negative capacitance and instability at electrified interfaces: Lessons from the study of membrane capacitors, Condensed matter physics **8**, 397 (2005).

[47] M. W. Hirsch, S. Smale, and R. L. Devaney, *Differential Equations, Dynamical Systems, and an Introduction to Chaos, 3rd Edition* (Academic Press, 2012).

[48] M. Orlik, *Self-Organization in Electrochemical Systems I* (Springer, 2012).

[49] A. Guerrero, J. Bisquert, and G. Garcia-Belmonte, Impedance spectroscopy of metal halide perovskite solar cells from the perspective of equivalent circuits, Chemical Reviews **121**, 14430 (2021).

[50] A. Lasia, *Electrochemical Impedance Spectroscopy and its Applications* (Springer, 2014).

[51] V. Vivier and M. E. Orazem, Impedance Analysis of Electrochemical Systems, Chemical Reviews **122**, 11131 (2022).

[52] D. E. Root and B. Hughes, in *32nd ARFTG Conference Digest*1988), pp. 1.

[53] J. C. Pedro, D. E. Root, J. Xu, and L. C. Nunes, *Nonlinear Circuit Simulation and Modeling: Fundamentals for Microwave Design* (Cambrige UP, 2018).

[54] J. Bisquert, A. Bou, A. Guerrero, and E. Hernández-Balaguera, Resistance transient dynamics in switchable perovskite memristors, APL Machine Learning **1**, 036101 (2023).

[55] E. Hernández-Balaguera, L. Munoz-Diaz, A. Bou, B. Romero, B. Ilyassov, A. Guerrero, and J. Bisquert, Long-Term Potentiation Mechanism of Biological

Postsynaptic Activity in Neuro-Inspired Halide Perovskite Memristors, Neuromorphic Computing and Engineering **3**, 024005 (2023).

[56] J. Cervera, M. Levin, and S. Mafe, Bioelectricity of non-excitable cells and multicellular pattern memories: Biophysical modeling, Phys. Rep. **1004**, 1 (2023).

[57] J. Cervera, M. Levin, and S. Mafe, Bioelectrical Coupling of Single-Cell States in Multicellular Systems, J. Phys. Chem. Lett. **11**, 3234 (2020).

[58] J. Bisquert, Device physics recipe to make spiking neurons Chemical Physics Reviews **4**, 10.1063/5.0145391 (2023).

[59] W. Z. Shen and A. G. U. Perera, Effect of interface states on negative capacitance characteristics in GaAs homojunction far-infrared detectors, Appl. Phys. A **72**, 107 (2001).

[60] J. Werner, A. F. J. Levi, R. T. Tung, M. Anzlowar, and M. Pinto, Origin of the excess capacitance at intimate Scottky contacts, Phys. Rev. Lett. **60**, 53 (1988).

[61] X. Wu, E. S. Tyang, and H. L. Evans, negative capacitance at metal-semiconductor contacts, J. Appl. Phys. **68**, 2845 (1990).

[62] E. Ehrenfreund, C. Lungenschmied, G. Dennler, H. Neugebauer, and N. S. Sariciftci, Negative capacitance in organic semiconductor devices: Bipolar injection and charge recombination mechanism, App. Phys. Lett. **91**, 012112 (2007).

[63] Q. Guo, N. Wang, and G. Zhang, A novel current-controlled memristor-based chaotic circuit, Integration **80**, 20 (2021).

[64] A. G. Alharbi, M. E. Fouda, Z. J. Khalifa, and M. H. Chowdhury, Electrical Nonlinearity Emulation Technique for Current-Controlled Memristive Devices, IEEE Access **5**, 5399 (2017).

[65] S. Kvatinsky, E. G. Friedman, A. Kolodny, and U. C. Weiser, TEAM: ThrEshold Adaptive Memristor Model, IEEE Transactions on Circuits and Systems I: Regular Papers **60**, 211 (2013).

[66] B. Muthuswamy *et al.*, in *2014 IEEE International Symposium on Circuits and Systems (ISCAS)*2014), pp. 490.

[67] J. Bisquert, Electrical Charge Coupling Dominates the Hysteresis Effect of Halide Perovskite Devices, J. Phys. Chem. Lett. **14**, 1014 (2023).

[68] C. Gonzales, A. Guerrero, and J. Bisquert, Transition from capacitive to inductive hysteresis: A neuron-style model to correlate I-V curves to impedances of metal halide perovskites, J. Phys. Chem. C **126**, 13560 (2022).

[69] A. T. P. Nicolae Filipoiu, Dragos-Victor Anghel, Roxana Patru, Rachel Elizabeth Brophy, Movaffaq Kateb, Cristina Besleaga, Andrei Gabriel Tomulescu, Ioana Pintilie, Andrei Manolescu, and George Alexandru Nemnes, Capacitive and inductive effects in perovskite solar cells: The different roles of ionic current and ionic charge

accumulation, Phys. Rev. Appl. **18**, 064087 (2022).

[70] V. Lopez-Richard, R. S. Wengenroth Silva, O. Lipan, and F. Hartmann, Tuning the conductance topology in solids, J. Appl. Phys. **133**, 134901 (2023).

[71] R. S. W. Silva, F. Hartmann, and V. Lopez-Richard, The Ubiquitous Memristive Response in Solids, IEEE Transactions on Electron Devices **69**, 5351 (2022).

[72] M. P. Sah, C. Yang, H. Kim, B. Muthuswamy, J. Jevtic, and L. Chua, A Generic Model of Memristors With Parasitic Components, IEEE Transactions on Circuits and Systems I: Regular Papers **62**, 891 (2015).

[73] S. Kumar, X. Wang, J. P. Strachan, Y. Yang, and W. D. Lu, Dynamical memristors for higher-complexity neuromorphic computing, Nat. rev. Mater. **7**, 575 (2022).

[74] A. Bou and J. Bisquert, Impedance spectroscopy dynamics of biological neural elements: from memristors to neurons and synapses, J. Phys. Chem. B **125** 9934 (2021).

[75] J. Bisquert, A frequency domain analysis of excitability and bifurcations of Fitzhugh-Nagumo neuron model., J. Phys. Chem. Lett. **12**, 11005 (2021).

[76] J. Bisquert and A. Guerrero, Dynamic Instability and Time Domain Response of a Model Halide Perovskite Memristor for Artificial Neurons, J. Phys. Chem. Lett. **13**, 3789 (2022).

[77] S. H. Strogatz, *Nonlinear Dynamics and Chaos, 2nd ed.* (CRC Press, 2019).

[78] E. Schöll, *Nonlinear Spatio-Temporal Dynamics and Chaos in Semiconductors* (Cambridge University Press, 2001).

[79] S. K. Scott, *Chemical Chaos* (Clarendon Press, 1991).

[80] W. Tress, J. P. Correa Baena, M. Saliba, A. Abate, and M. Graetzel, Inverted Current–Voltage Hysteresis in Mixed Perovskite Solar Cells: Polarization, Energy Barriers, and Defect Recombination, Adv. Energy Mater. **6**, 1600396 (2016).

[81] O. Gharbi, M. T. T. Tran, B. Tribollet, M. Turmine, and V. Vivier, Revisiting cyclic voltammetry and electrochemical impedance spectroscopy analysis for capacitance measurements, Electrochimica Acta **343**, 136109 (2020).

[82] M. D. Pickett, D. B. Strukov, J. L. Borghetti, J. J. Yang, G. S. Snider, D. R. Stewart, and R. S. Williams, Switching dynamics in titanium dioxide memristive devices, J. Appl. Phys. **106**, 074508 (2009).

[83] M. Berruet, J. C. Pérez-Martínez, B. Romero, C. Gonzales, A. M. Al-Mayouf, A. Guerrero, and J. Bisquert, Physical model for the current-voltage hysteresis and impedance of halide perovskite memristors, ACS Energy Lett. **7**, 1214 (2022).

[84] L. Munoz-Diaz, A. J. Rosa, A. Bou, R. S. Sanchez, B. Romero, R. A. John, M. V. Kovalenko, A. Guerrero, and J. Bisquert, Inductive and Capacitive Hysteresis of Halide Perovskite Solar Cells and Memristors Under Illumination, Frontiers in Energy

Research **10**, 914115 (2022).

[85] D. Wang, W. Brown, Y. Li, M. Kvetny, J. Liu, and G. Wang, Correlation of Ion Transport Hysteresis with the Nanogeometry and Surface Factors in Single Conical Nanopores, Analytical Chemistry **89**, 11811 (2017).

[86] E. J. Juarez-Perez, R. S. Sanchez, L. Badia, G. Garcia-Belmonte, V. Gonzalez-Pedro, Y. S. Kang, I. Mora-Sero, and J. Bisquert, Photoinduced giant dielectric constant in lead halide perovskite solar cells, J. Phys. Chem. Lett. **5**, 2390−2394 (2014).

[87] Brett C. Carter, Andrew J. Giessel, Bernardo L. Sabatini, and Bruce P. Bean, Transient Sodium Current at Subthreshold Voltages: Activation by EPSP Waveforms, Neuron **75**, 1081 (2012).

[88] H. Bao, C. Chen, Y. Cao, S. Chang, S. Wang, and H. Zhong, Quantitative Determination of Charge Accumulation and Recombination in Operational Quantum Dots Light Emitting Diodes via Time-Resolved Electroluminescence Spectroscopy, J. Phys. Chem. Lett., 1777 (2023).

[89] J. G. Simmons, Generalized formula for the electric tunnel effect between similar electrodes separated by a thin insulating film, J. Appl. Phys. **34**, 1793 (1963).

[90] V. J. Francis, *Fundamentals of Discharge Tube Circuits.* (Methuen, 1948).

[91] D. Klotz, Negative capacitance or inductive loop? – A general assessment of a common low frequency impedance feature, Electrochem. Comm. **98**, 58 (2019).

[92] S. Fletcher, Tables of Degenerate Electrical Networks for Use in the Equivalent-Circuit Analysis of Electrochemical Systems, J. Electrochem. Soc. **141**, 1823 (1994).

[93] K. Sun, J. Chen, and X. Yan, The Future of Memristors: Materials Engineering and Neural Networks, Adv. Func. Mater. **31**, 2006773 (2021).

[94] L. Chua, Memristor-The missing circuit element, IEEE Transactions on Circuit Theory **18**, 507 (1971).

[95] C. Gonzales, A. Guerrero, and J. Bisquert, Spectral properties of the dynamic state transition in metal halide perovskite-based memristor exhibiting negative capacitance, App. Phys. Lett. **118**, 073501 (2021).